

Comprehensive Computational Analysis of Protein Phenotype Changes Due to Plausible Deleterious Variants of Human SPTLC1 Gene

Tayyaba Sadaf, Peter John*, Attiya Bhatti

Department of Health Care Biotechnology, Atta-ur-Rahman School of Applied Biosciences (ASAB), National University of Sciences and Technology (NUST), Islamabad, Pakistan.

Submitted 18 October 2018; Accepted 12 April 2019; Published 23 April 2019

Genetic variations found in the coding and non-coding regions of a gene are known to influence the structure as well as the function of proteins. Serine palmitoyltransferase long chain subunit 1 a member of α -oxoamine synthase family is encoded by *SPTLC1* gene which is a subunit of enzyme serine palmitoyltransferase (SPT). Mutations in *SPTLC1* have been associated with hereditary sensory and autonomic neuropathy type I (HSAN-I). The exact mechanism through which these mutations elicit protein phenotype changes in terms of structure, stability and interaction with other molecules is unknown. Thus, we aimed to perform a comprehensive computational analysis of single nucleotide polymorphisms (SNPs) of *SPTLC1* to prioritize a list of potential deleterious SNPs and to investigate the protein phenotype change due to functional polymorphisms. In this study, a diverse set of *SPTLC1* SNPs were collected and scrutinized to categorize the potential deleterious variants. Our study concordantly identified 21 non-synonymous SNPs as pathogenic and deleterious that might induce alterations in protein structure, flexibility and stability. Moreover, evaluation of frameshift, 3' and 5' UTR variants shows c.*1302T>G as effective. This comprehensive *in silico* analysis of systematically characterized list of potential deleterious variants could open avenues as primary filter to substantiate plausible pathogenic structural and functional impact of variants.

Key words: Single nucleotide polymorphisms, computational, deleterious, variants, bioinformatics tools

Sphingolipids belong to a diverse family of cellular lipids that perform fundamental functions both as membrane components and as signaling molecules (1). Cells obtain sphingolipids intrinsically by *de novo* biosynthesis and extrinsically by up-take and reusing the exogenous sphingolipids (1). An endoplasmic reticulum-confined enzyme, serine palmitoyltransferase

(SPT), is a pyridoxal 5'-phosphate dependent multimeric enzyme, which acts as a vital player for *de novo* biosynthesis of sphingolipids. This enzyme catalyzes the foremost step of sphingolipid metabolism i.e., the condensation of L-serine and palmitoyl coenzyme (CoA) for producing 3-ketodihydrosphingosine (KSD) (2, 3). The activity of SPT in *de novo* sphingolipid biosynthesis

*Corresponding author: Department of Health Care Biotechnology, Atta-ur-Rahman School of Applied Biosciences (ASAB), National University of Sciences and Technology (NUST), Islamabad, Pakistan. Email: pjohn@asab.nust.edu.pk

pathway is required for various normal cellular functions including the survival of adipocyte cells. The decreased *de novo* sphingolipid biosynthesis inside adipocytes leads to adipocyte death, adipose tissue remodeling, and metabolic disorder (4).

An important SPT subunit, SPT long chain subunit 1 encoded by *SPTLC1* gene is the member of -oxoamine synthase family (5). It is mapped to chromosome 9q22.1-q22.3, and contains 15 exons that encode for a protein with 473 amino acid residues (6). The structure and function of SPT is usually disturbed by mutations in *SPTLC1* gene, which occur at amino acids that are highly conserved throughout various species (7). Mutations in *SPTLC1* have been associated with hereditary sensory and autonomic neuropathy type I (HSAN-I) (6, 8). HSAN-I is an autosomal predominant dynamic degenerative hereditary disorder of peripheral sensory neurons characterized by dorsal root ganglia (DRG) and motor neurons degeneration. It is the most common subtype of HSAN or hereditary sensory neuropathy (HSN). In HSAN-I, the enzymatic selectivity of mutant SPT is lost and L-alanine is utilized as an alternative substrate, which results in the formation of atypical and neurotoxic 1-deoxy-sphingolipids (9, 10). This promiscuous enzymatic activity of mutant SPT is suggested to be the pathological reason of HSAN-I (11, 12). A noticeable rise in endoplasmic reticulum (ER) stress has also been observed in HSAN-I patient cells, expressing the p.V144D mutant SPTLC1 protein as compared to cells of healthy controls (13). The protein modifications reflect the altering cellular events that bring about HSAN-I. Recently, a notable change in the expression of a group of proteins in the mitochondria and ER has been detected in SPTLC1 p.V144D mutant lymphoblasts (14-16). Notably, identified changes also exhibited in the p.C133W and p.C133Y mutations (17).

During recent years, there has been extensive consideration in associating the genetic variations

to protein phenotype changes. However, determining the disease-associated missense mutations had been a challenging task for genetic disorder research. Owing to the significance of *SPTLC1* mutations and its subsequent link with a spectrum of clinical pathologies, this study has intended to investigate the disease causal mutations in exonic and regulatory regions (5' and 3' UTRs) to develop the predictions and facilitate their pathogenic characterization based on their impact to structure and function of SPTLC1 protein. Thus, we implemented computational approach for screening the possible detrimental mutations of *SPTLC1* and computationally analyzed structural and functional impact of screened potential mutations.

Material and methods

Collection of dataset

The *SPTLC1* polymorphisms data belong to NM_006415.2 transcript and NP_006406.1 amino acid sequence was mined from databases including NCBI (National Centre for Biotechnology Information) affiliated dbSNP(18) and exome variant server (Server EV. NHLBI GO exome sequencing project (ESP)). Concerned protein sequence and information was retrieved from Ensembl (19) (ENSG00000090054; ENSP00000262554), OMIM (Online Mendelian Inheritance in Man) (20) and UniProt (UniProt Consortium, 2015) (O15269), that provide ample high-quality sequence and functional information of protein for our computational analysis. Redundant mutations obtained from various sources were eliminated to reform the data. Based on variants nature and position, data was classified as missense, insertion and deletions, frameshift and untranslated regions (Fig. 1A).

Analysis of variants at genomic level

Prediction of nsSNPs having structural and functional impact

To predict important SNPs influencing a protein upon substitution functionally, servers like

Sorting Intolerant from Tolerant (SIFT), Polymorphism Phenotyping v2 (PolyPhen-2), Protein Variation Effect Analyzer (PROVEAN) and MutPred were used. These servers provide rapid analysis of variants supporting high-throughput investigation at genetic and protein level. Firstly, the variants were assessed by a sequence homology-based program SIFT (21-23). If the score of the variant was less than a chosen threshold (0.05), the variant was classified as deleterious and vice versa. Physiochemical differences, evolutionary conservation, and substitution proximity to the structural level alterations of protein upon substitution were identified by PolyPhen-2 (24). The variant was categorized as “probably damaging” by PolyPhen-2, if the position-specific independent count (PSIC) score was 0.99-1.00, and “possible damaging” if the score was 0.50-0.99, and the rest were categorized as “benign” (with no phenotypic influence). Biological functional changes of a protein due to a variant were also computed by PROVEAN that worked on sequence clustering and alignment-based scoring. The variant was classified as deleterious if the prediction score was <-2.5 (25, 26), according to PROVEAN program. To examine whether the molecular variance was involved in insurgence of human diseases, the impact of variants was also estimated by web-based tool MutPred (27).

Indels, frameshift and UTR variants analysis

The detrimental nature of insertions, deletions and frameshift mutations were predicted by SIFT Indel Classifier that requires comma separated list of chromosome coordinates, orientation (1, -1) and indels as input (28). Functionally important indels were also filtered by PROVEAN. The indels were considered deleterious if the score was <=-2.5 and neutral if the variant score was > -2.5 (25, 26). Functional sequence pattern positioned in 5' and 3' UTR sequences were collected from dbSNP (18) and specialized untranslated regions of eukaryotic mRNAs databases: UTRdb and UTR site (29, 30).

These variants were analyzed by UTR specific tool UTRScan. User submitted sequences were carefully searched by UTRScan for any functional elements or patterns endorsed by UTRsite and UTR database.

Analysis of variants at structural level

Modeling of SPTLC1 protein structure

The human SPTLC1 protein sequence comprising 473 amino acid residue was subjected to SWISS-MODEL (31-34) for homology modeling. Evaluation of modeled structure was carried out using ERRAT (35), RAMPAGE (36) and ProSA-web (37) servers. The structure was passed through energy minimization step to remove the internal constraints with GROMOS96 implementation of Swiss-PdbViewer 4.1.0 after adding hydrogen atoms (38).

Analysis of protein characteristics properties

MUpro server was used to find out the effect of non-synonymous SNPs (nsSNPs) on protein stability. The predicted score less than 0 shows decrease in protein stability due to the mutation; contrariwise, a score greater than 0 refers to an increase in protein stability (39). Solvent accessibility of structures was predicted by an artificial neural network-based program NetSurfP-1.1 (40) and Predict Protein (41). For approximating residue specific quality of protein structure prediction and the inherent B-factor profile of all residues along the chain by combining local structure assembly variations with sequence- and structure-based profilingResQ server was used (42).

Functional analysis of mutations

Multi-scale binding pockets on SPTLC1 protein surface were explored by GHECOM 1.0: Grid-based HECOMi finder server (43). Functional association of SPTLC1 protein was critically assessed using the Search Tool for the Retrieval of Interacting Genes (STRING) v10 database (44). Protein-Protein interaction of SPTLC1 including both physical and functional associations based on known interactions (curated and experimentally determined), predicted interactions (gene

neighborhood, gene fusions and gene co-occurrence), text mining, co-expression and protein homology was identified. The edges of network represent the association between nodes (interacting proteins).

Protein-protein docking simulation

A flexible protein docking approach, the HADDOCK (High Ambiguity Driven protein-protein DOCKing) version 2.2 (45) was used to perform modeling of biomolecular complex: SPTLC1 with its highest interacting partner. The identification of active and passive residues of interacting biomolecules was performed by CPORT (46).

Results

Mutation spectrum of *SPTLC1* gene

The examined gene comprises a total of 273 human SNPs belonging to different classes of mutations including synonymous and non-synonymous. Among all the included mutations in our study, missense mutations seemed to be the most abundant mutations with $n = 168$ (61.5%) when compared to indels ($n = 3$), frameshift ($n = 9$), and UTRs ($n = 94$; 34.4%) (Fig. 1A). Noticeable uneven distribution of mutations in exons is represented in Fig. 1B.

Analysis at genomic level

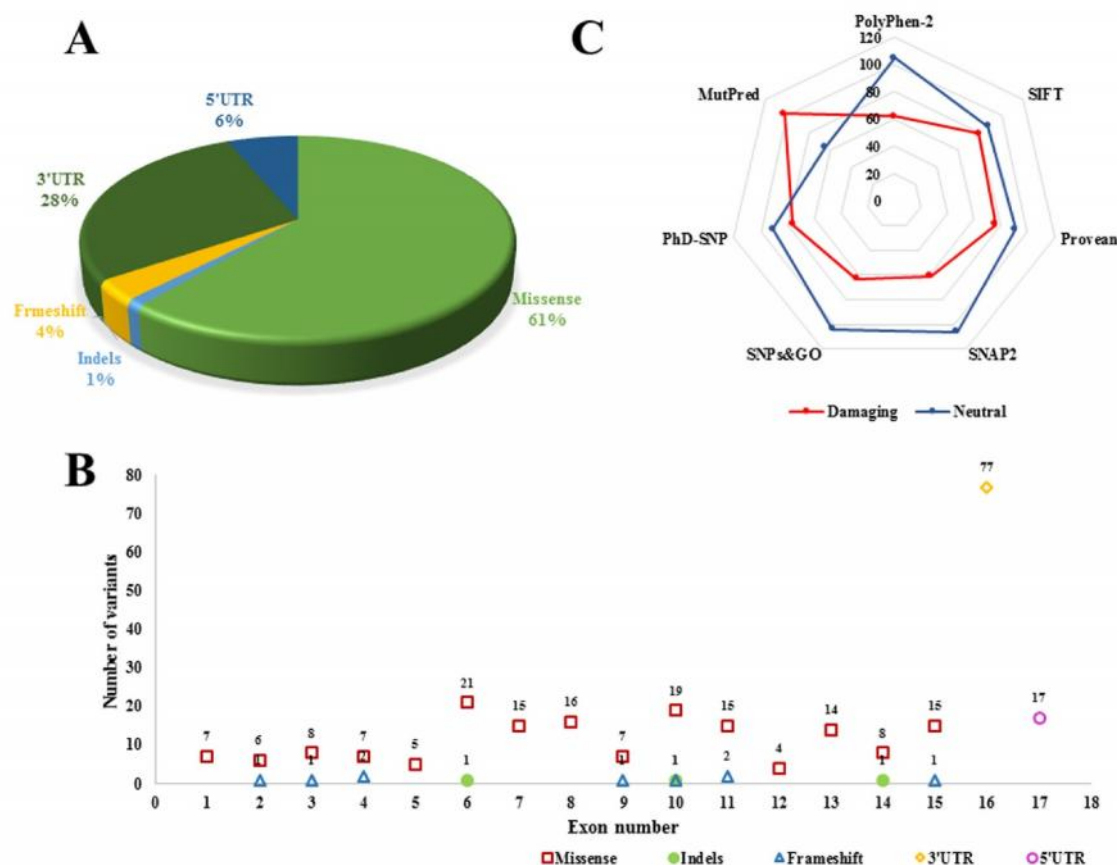


Fig. 1. Distribution of *SPTLC1* nucleotide variants. A: pie chart representing different classes of mutations; B: scatter plot representing the number of missense, indels, frameshift mutations per exon and number of 3'UTR and 5'UTR variants; C: radar chart representing the total number of pathogenic and neutral *SPTLC1* variants by each prediction program..

Table 1. List of selected SPTLC1 missense variants with their corresponding exon, chromosome position and protein variants with predicted scores by SIFT, PolyPhen-2, PROVEAN, MutPred and MUpro.

S. No.	NT Variant	Ex on	Chr. position	PRO Variant	PolyPhen-2		SIFT		PROVEAN		Mut-Pred PR	MUpro
					Pred	Score	Pred	Score	Pre d	Score		
1	310G>A	4	92080914	104A>T	pr dmg	0.998	dmg	0.01	del	-3.079	0.779	-1.2661182
2	325C>G	4	92080899	109L>V	pr dmg	0.989	dmg	0.01	del	-2.901	0.856	-1.0533436
3	398G>A	5	92080045	133C>Y	pr dmg	1	dmg	0	del	-10.725	0.839	-0.282728
4	399T>G	5	92080044	133C>W	pr dmg	1	dmg	0	del	-10.726	0.853	-0.31455734
5	431T>A	6	92068095	144V>D	pr dmg	0.998	dmg	0	del	-6.207	0.871	-1.9523302
6	457G>A	6	92068069	153A>T	pos dmg	0.882	dmg	0	del	-3.584	0.901	-1.3441989
7	481G>A	6	92068045	161A>T	poss dmg	0.87	dmg	0	del	-3.411	0.796	-1.2131073
8	485T>G	6	92068041	162I>S	pr dmg	0.996	dmg	0	del	-5.365	0.772	-2.3519006
9	524T>C	6	92068002	175I>T	pr dmg	0.999	dmg	0	del	-4.698	0.784	-1.8899242
10	563A>C	7	92059306	188D>A	pr dmg	0.988	dmg	0.01	del	-7.484	0.895	-0.97234279
11	743A>G	8	92055442	248Y>C	benign	0.053	dmg	0	del	-7.668	0.771	-0.67134313
12	832T>G	9	92050016	278S>A	poss dmg	0.59	TOL	0.07	del	-2.641	0.845	-1.2437183
13	929C>G	10	92047668	310A>G	benign	0.006	dmg	0.02	del	-2.824	0.832	-1.4961316
14	946G>A	10	92047651	316G>S	pr dmg	0.993	dmg	0.01	del	-5.191	0.927	-1.3775049
15	952T>A	10	92047645	318C>S	pr dmg	0.989	TOL	0.05	del	-8.278	0.808	-0.56363416
16	992C>T	11	92047261	331S>F	benign	0.222	dmg	0.03	del	-4.533	0.759	-0.67561754
17	992C>A	11	92047261	331S>Y	poss dmg	0.454	dmg	0	del	-4.50	0.825	-0.97224916
18	1055C>T	11	92047198	352A>V	benign	0.066	dmg	0.01	del	-2.909	0.857	-0.63107997
19	1160G>C	13	92038342	387G>A	benign	0.41	dmg	0.03	del	-3.117	0.817	0.07064886
20	1334G>A	15	92032553	445R>Q	pr dmg	0.998	dmg	0.01	del	-3.245	0.88	-1.3868538
21	1333C>T	15	92032554	445R>W	pr dmg	1	dmg	0	del	-6.841	0.874	-1.2548201

NT: nucleotide; Chr: chromosome; PRO: protein; Pred: prediction; Accu: accuracy; PR: probability; poss: possibility; dmg: damaging; TOL: tolerant; N: neutral; DIS: disease.

Analysis of deleterious missense mutations

Among the 168 missense mutations, SIFTanalysis revealed 80 (47.6%) nsSNPs as “damaging” or “intolerant” having a tolerance index score of 0.05, while 88 (52.3%) mutations were “tolerant” with > 0.05 score (Fig. 1C). Out of 80 damaging mutations, 33 (41.25%) and 24 (30%) nsSNPs were “extremely-intolerant” with 0.00 and 0.01 score, respectively and 23 (28.75%) nsSNPs were just “intolerant”. According to PolyPhen-v2 prediction, a total of 63 (37.5%) nsSNPs were expected to be damaging. Of which, 36 nsSNPs were “probably damaging” with score ranging from

0.99 to 1.00, and 27 were “possibly damaging” with score ranging from 0.5 to 0.9, and the remaining 105 nsSNPs were classified as benign. A total of 77 (45.8%) mutations were predicted deleterious and 91 (54.1%) were neutral by PROVEAN. Among all the deleterious mutations 54 (70.1%) were least deleterious, 23 (29.8%) were deleterious with score < -5.0, of which 2 mutations (p.C133CY and p.C133W) were deleterious with score < -10.0. About 104 (61.9%) and only 28 (16.66%) nsSNPs with > 0.5 and 0.75 probability score were predicted as disease associated mutations by MutPred. However, the concordant analysis

predicted 21 mutations mentioned in Table 1 as potential predicted mutations that can be deleterious. Protein stability analysis by MUpro

revealed that all the selected mutants would decrease the stability except p.G387A as the predicted score of all other mutants was less than

Table 2. SIFT indel classifier and PROVEAN prediction analysis for indels and frameshift variants.

Nucleotide variant	Coordinates	Subs. type	Exo n	AA variant	Clin. sig.	PROVEAN		SIFT	
						Score	Pred.	Score	Pred.
c.139delC	92112481	FS-del	2	Q47Kfs	NA	-	-	0.858	dam
c.174delA	92108826	FS-del	3	E59Nfs	NA	-	-	0.858	dam
c.281_282delTG	92080942:92080943	FS-del	4	V94Gfs	NA	-	-	0.858	dam
c.277_278insA	92080946:92080947	FS-ins	4	T93Nfs	NA	-	-	0.858	dam
c.452_454delGCC	92068072:92068074	del	6	R151del	NA	-12.837	dele	0.858	dam
c.804_805insTA	92050043:92050044	FS-in	9	A269Terfs	NA	-	-	0.858	dam
c.895_897delGAT	92047700:92047702	del	10	D299del	NA	-8.167	dele	0.529	dam
c.963_964insG	92047633:92047634	FS-ins	10	S322Vfs	NA	-	-	0.858	dam
c.1031delT	92047222	FS-del	11	L344Rfs	NA	-	-	0.858	dam
c.1029_1030delCC	92047223:92047224	FS-del	11	L344Vfs	NA	-	-	0.858	dam
c.1305_1307delAGA	92034831:92034833	del	14	E436del	NA	-1.925	N	0.858	dam
c.1361_1362delAG	92032525:92032526	FS-del	15	E454Gfs	NA	-	-	0.783	Dam

Subs. Type: substitution type; FS: frameshift; del: deletion; ins: insertion; Clin.sig.:clinical significance; Pred.: prediction; dele: deleterious; N: neutral; dam: damaging.

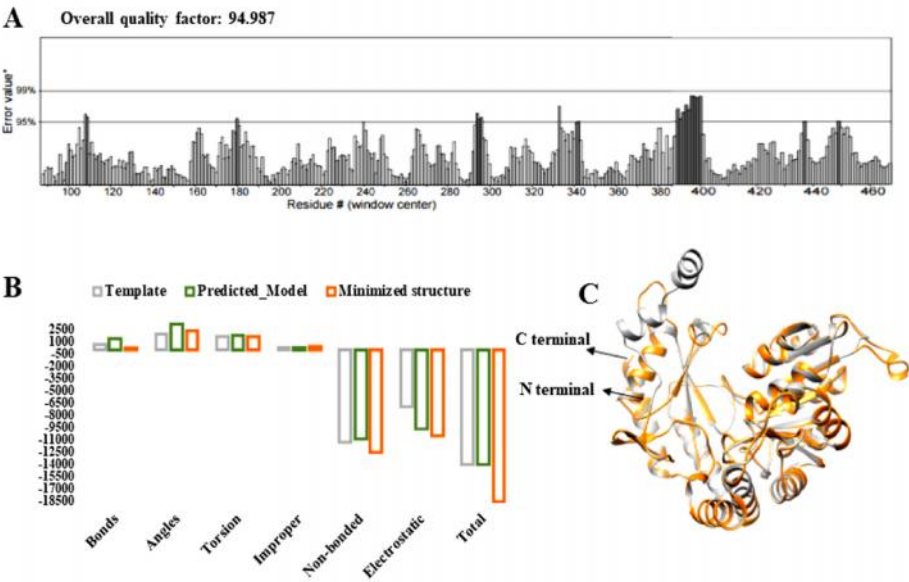


Fig. 2. Selected human SPTLC1 predicted protein structure evaluation and energy value representation. A: ERRAT indicates 94.987 overall quality factor; B: colored bars used for representing the computed energy values in KJ/mol of template and predicted model (grey color for template used for structure prediction, green color for predicted model before energy minimization, and orange color for predicted model after energy minimization step); C: superimposition of template 3a2b (grey) and predicted SPTLC1 structure (orange red) shows high structural similarity.

Table 3. UTRScan prediction result for 3'UTR variants of SPTLC1 protein (Transcript ID:NM_006415.2).

S.No.	rs ID	Position	Prediction	S.No.	rs ID	Position	Prediction
1	rs758071979	c.*10C>T	-	40	rs115637483	c.*490A>G	-
2	rs200727312	c.*11G>A	-	41	rs531407417	c.*494T>C	-
3	rs778790410	c.*13G>A	-	42	rs74939390	c.*525G>T	uORF [519,608]
4	rs756960214	c.*20G>C	uORF [17,109]	43	rs144733313	c.*569G>A	uORF [519,608]
5	rs753599241	c.*23T>C	uORF [17,109]	44	rs367609260	c.*581T>C	uORF [519,608]
6	rs867197507	c.*28C>T	uORF [17,109]	45	rs537125477	c.*590T>G	-
7	rs374737655	c.*31C>T	uORF [17,109]	46	rs773137233	c.*614C>T	-
8	rs760602474	c.*38C>T	uORF [17,109]	47	rs576072015	c.*654A>G	-
9	rs370307230	c.*39G>A	uORF [17,109]	48	rs765100762	c.*657A>C	-
10	rs202080725	c.*46A>C	uORF [17,109]	49	rs761445360	c.*664C>G	-
11	rs550740752	c.*46G>A	uORF [17,109]	50	rs189417944	c.*670G>A	-
12	rs763262266	c.*50T>C	uORF [17,109]	51	rs866982133	c.*711T>G	uORF [705,782]
13	rs773269599	c.*58C>T	uORF [17,109]	52	rs142008725	c.*713A>C	uORF [705,782]
14	rs535778954	c.*60C>T	uORF [17,109]	53	rs879644362	c.*745C>G	uORF [705,782]
15	rs73653020	c.*61G>A	uORF [17,109]	54	rs768395365	c.*750C>T	uORF [705,782]
16	rs777118329	c.*68A>G	uORF [17,109]	55	rs568268325	c.*809T>C	-
17	rs1131864	c.*78C>T	uORF [17,109]	56	rs527344506	c.*822C>T	-
18	rs769349062	c.*95C>T	uORF [17,109]	57	rs374347262	c.*828T>G	uORF [827,1057]
19	rs1131866	c.*102A>G	uORF [17,109]	58	rs760223808	c.*864C>T	uORF [827,1057]
20	rs7024575	c.*112G>A	-	59	rs535318963	c.*867G>A	uORF [827,1057]
21	rs189582528	c.*124A>G	-	60	rs570805058	c.*875A>T	uORF [827,1057]
22	rs771433261	c.*133A>G	uORF [125,250]	61	rs570164486	c.*916A>G	uORF [827,1057]
23	rs745563960	c.*144A>G	uORF [125,250]	62	rs775237786	c.*932A>G	uORF [827,1057]
24	rs544879549	c.*147G>A	uORF [125,250]	63	rs771458551	c.*983T>C	uORF [827,1057]
25	rs184220566	c.*178T>A	uORF [125,250]	64	rs559735773	c.*1009G>T	uORF [827,1057]
26	rs552433019	c.*190A>C	uORF [125,250]	65	rs530944752	c.*1015G>A	uORF [827,1057]
27	rs753700526	c.*196A>G	uORF [125,250]	66	rs367968859	c.*1034T>C	uORF [827,1057]
28	rs377023278	c.*217T>A	uORF [125,250]	67	rs766363634	c.*1046T>C	uORF [827,1057]
29	rs531033514	c.*228A>G	uORF [125,250]	68	rs145019674	c.*1052A>G	uORF [827,1057]
30	rs563505829	c.*272A>G	-	69	rs77041650	c.*1067C>T	uORF [1063,1158]
31	rs766183581	c.*290T>C	ORF [281,376]	70	rs548652432	c.*1068A>G	uORF [1063,1158]
32	rs542032121	c.*320G>A	ORF [281,376]	71	rs142740904	c.*1154T>C	uORF [1063,1158]
33	rs564259149	c.*334C>G	ORF [281,376]	72	rs112076327	c.*1170T>C	-
34	rs529884120	c.*401C>A	-	73	rs760602744	c.*1209G>A	uORF [1177,1242]
35	rs372012368	c.*402A>T	-	74	rs541013337	c.*1221C>T	uORF [1177,1242]
36	rs7944	c.*445A>G	uORF [410,478]	75	rs562277733	c.*1226G>T	uORF [1177,1242]
37	rs868416931	c.*451G>T	uORF [410,478]	76	rs530126189	c.*1230G>A	uORF [1177,1242]
38	rs541284488	c.*483A>G	-	77	rs7035964	c.*1302T>G	CPE [1290,1339], IRES [1243,1339], uORF [1265,1333], PAS [1300,1339]
39	rs181586912	c.*488G>T	-				

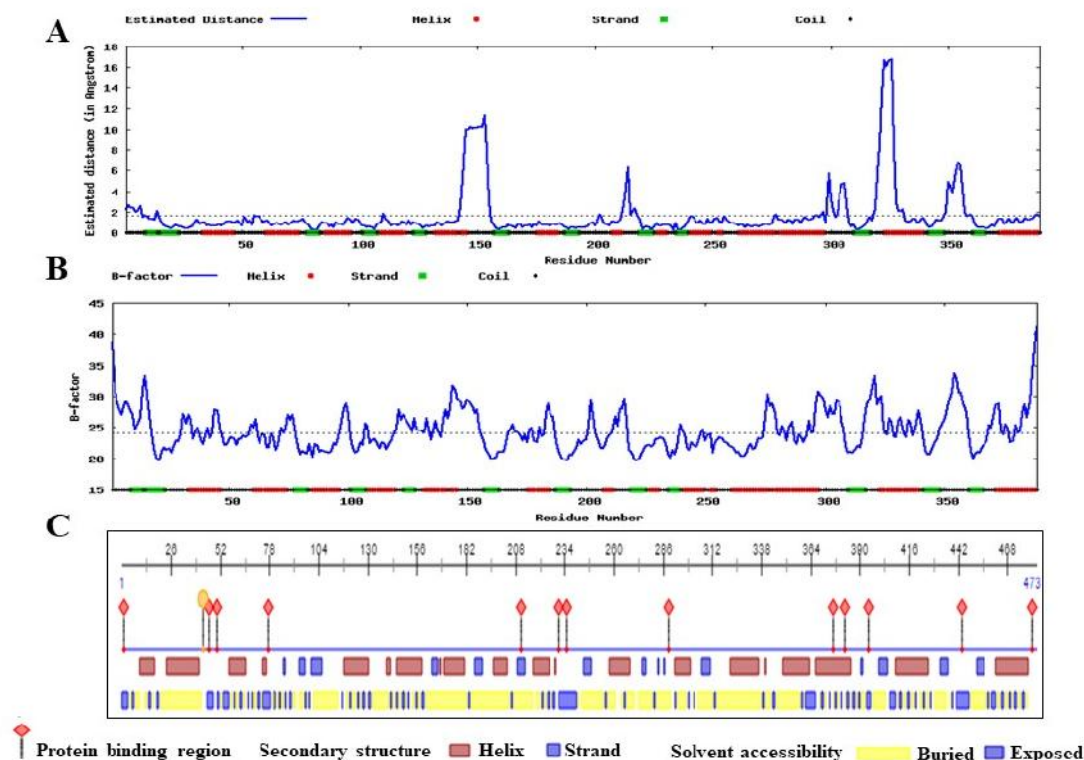


Fig. 3. Analysis of protein properties. A: secondary structure and solvent accessibility analysis by PredictProtein; B: the local quality defined as the distance deviation (in Angstrom) between residue positions in the model and the native structure; C: stability of different parts of the structure in terms of beta factor by ResQ server.

Table 4. UTRScan prediction result for 5'UTR variants of SPTLC1 protein.

S.No.	rs ID	Transcript ID	Position	Prediction
1	rs750255730	NM_006415.2	c.-3A>G	-
2	rs758217796	NM_006415.2	c.-6C>A	-
3	rs746676272	NM_006415.2	c.-7G>T	-
4	rs754378890	NM_006415.2	c.-10G>C	-
5	rs780821663	NM_006415.2	c.-19C>T	-
6	rs558203491	NM_006415.2	c.-27C>T	-
7	rs770382920	NM_006415.2	c.-28C>A	-
8	rs201897322	NM_006415.2	c.-29A>C	-
9	rs773682043	NM_006415.2	c.-34T>C	-
10	rs866449132	NM_006415.3	c.-39C>A	-
11	rs749631140	NM_006415.3	c.-49A>G	-
		NM_006415.3	c.-49A>T	-
12	rs774659397	NM_178324.2	c.-51G>A	-
13	rs55740103	NM_006415.3	c.-64T>C	-
14	rs552690353	NM_178324.2	c.-70C>T	-
15	rs184693119	NM_006415.3	c.-76T>C	-
16	rs111298150	NM_006415.3	c.-96C>T	-
17	rs557306141	NM_178324.2	c.-103G>T	-

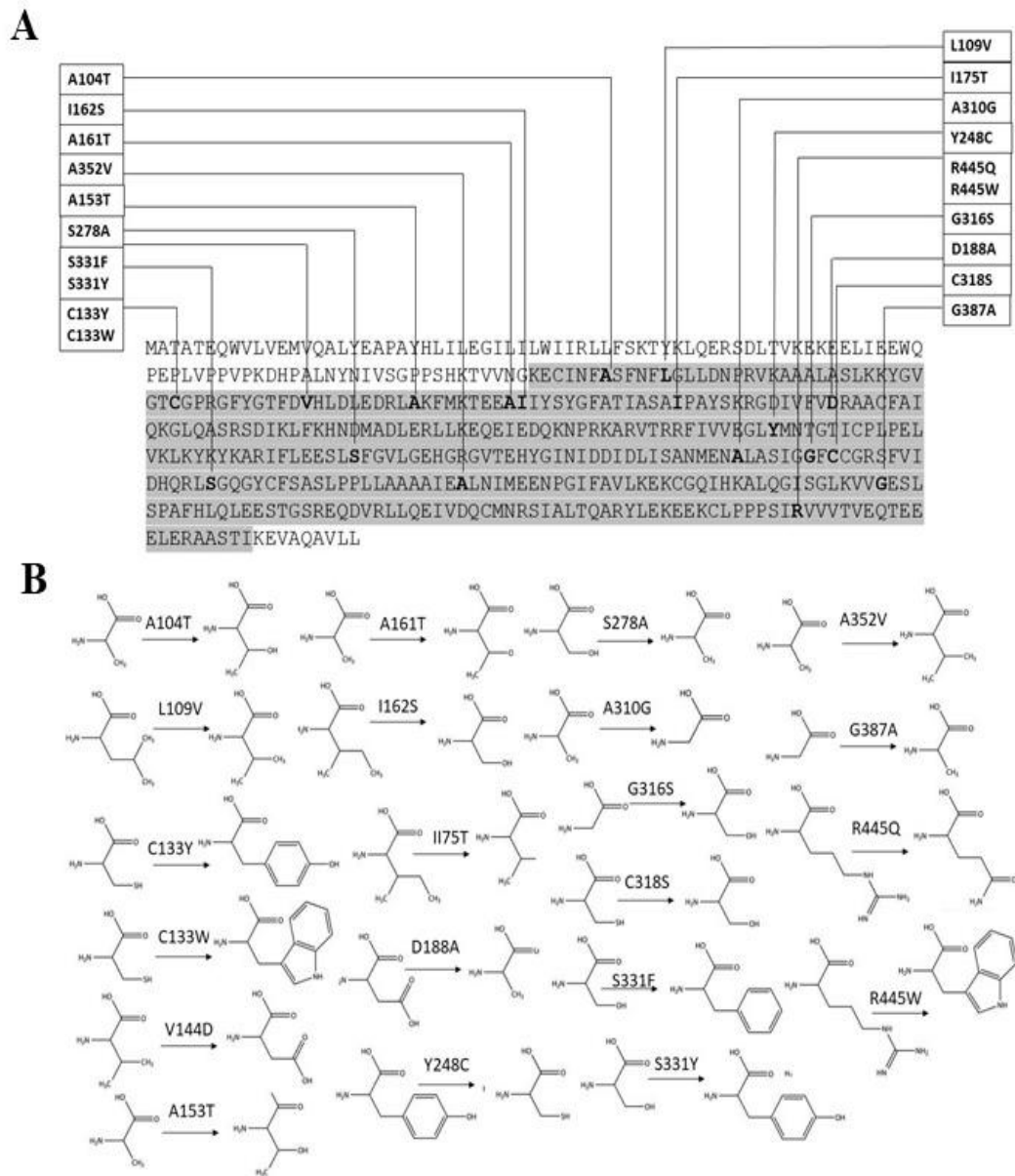


Fig. 4. Protein mutations analysis. A: 21 identified mutations in the protein sequence showed that all the predicted mutations belong to the serine C-palmitoyltransferase activity domain of the protein; B: structural differences between selected wild type and mutant residues of SPTLC1 protein.

zero (Table 1).

Indel, frameshift and UTR variants analysis

A total of 94 UTR variants were identified. Out of which 17 variants were lying in 5' UTR and 77 in 3' UTR sequences (Tables 3 and 4). The UTRscan identified that 21 variant had no effect, but 55 variants were lying in the region important for open reading frame (ORF) and 1 variant c.*1302T>G in 3'UTR was found in the region

associated with polyadenylation signal (PAS), cytoplasmic polyadenylation (CPE), internal ribosomal entry site (IRES) (Table 3).

SPTLC1 structural analysis

3D structure modeling and evaluation

Native human SPTLC1 model built by homology modeling based on 3a2b.1.A template showed the good overall quality and stereochemical properties suggesting a reliable structure

(Fig. 2). The whole structure was modeled from 83-471 residues and consisted of 17 alpha and 12 beta sheets. RAMPAGE showed 376 (97.2%) residues in favored region, 9 (2.3%) in allowed region, and only 2 (0.5%) residues (Ala172 and Lys268) as

outliers. However, the local model quality estimated by PROSA-web calculated the energies of residues as negative and the overall quality model of the predicted structure indicated the -9.24 z-score that lies within the characteristic range.

Table 5. Surface accessibility prediction scores by NetSurfP and ResQ web server for models.

Position	Residue	RSA	ASA	Z-score	Class assigned	rBF	nBF
104	A	0.022	2.402	0.215	B	21.03	-0.38
	T	0.031	4.244	-0.356	B	-	-
109	L	0.089	16.296	-0.912	B	22.39	-0.21
	V	0.086	13.234	-0.852	B	-	-
133	C	0.2	28.108	-2.467	B	23.41	-0.08
	Y	0.22	46.993	-2.339	B	-	-
	W	0.182	43.867	-2.631	B	-	-
144	V	0.117	17.937	0.914	B	23.54	-0.06
	D	0.105	15.188	0.997	B	-	-
153	A	0.128	14.128	0.525	B	22.14	-0.24
	T	0.156	21.609	0.577	B	-	-
161	A	0.017	1.840	0.828	B	21.90	-0.27
	T	0.018	2.441	0.737	B	-	-
162	I	0.033	6.105	0.675	B	20.65	-0.27
	S	0.035	4.102	0.607	B	-	-
175	I	0.044	8.214	0.470	B	21.16	-0.36
	T	0.047	6.477	0.275	B	-	-
188	D	0.085	12.220	-0.493	B	22.10	-0.24
	A	0.072	7.912	-0.395	B	-	-
248	Y	0.087	18.656	-0.160	B	22.43	-0.20
	C	0.092	12.917	-0.080	B	-	-
278	S	0.040	4.676	-1.360	B	21.67	-0.30
	A	0.040	4.419	-1.457	B	-	-
310	A	0.047	5.223	-2.633	B	22.10	-0.24
	G	0.045	3.534	-2.626	B	-	-
316	G	0.028	2.196	-1.564	B	20.77	-0.41
	S	0.034	3.973	-2.044	B	-	-
318	C	0.045	6.290	-0.178	B	21.33	-0.34
	S	0.037	4.301	-0.952	B	-	-
331	S	0.360	42.227	-0.624	E	24.66	0.07
	F	0.360	72.352	-0.700	E	-	-
	Y	0.376	80.394	-1.037	E	-	-
352	A	0.025	2.799	0.332	B	21.44	-0.33
	V	0.025	3.873	0.234	B	-	-
387	G	0.311	24.460	-1.840	B	29.44	0.67
	A	0.340	26.750	-1.867	E	-	-
445	R	0.041	9.389	0.259	B	20.76	-0.41
	Q	0.043	7.662	0.338	B	-	-
	W	0.047	11.328	0.068	B	-	-

RSA: relative surface area (value <0.2 (buried residues); > 0.2 (exposed residues). ASA: absolute surface area (value <25% of ASA_{max}(buried); value > 25% of ASA_{max}(exposed)); B: buried or E: exposed; rBF: raw beta factor; nBF: normalized beta factor.

Protein characteristic properties analysis

In our analysis, PredictProtein predicted that most of the residues were in buried region (Fig. 3A). Thus, we employed NetSurfP server. Most of the identified mutant residues belonged to the buried region of protein (Table 5) except Ser331. Moreover, the estimated local quality defined as the distance deviation between native and model protein residual position using support vector regression showed that most of the residues were below the cut-off value (Fig. 3B). The stability and flexibility of different parts of the model evaluated by ResQ server depicted that most of the residues belonged to the well-order structure of the protein as the calculated raw and normalized beta factor values were less than the cut-off score (Fig. 3C and Table 5). It has been observed that the mutated residues belonged to the serine C-palmitoyltransferase activity domain (Fig. 4A). Also, structural difference of amino acids revealed that substituted residues have explicit properties like size, shape, density and charges (Fig. 4B), thus

would impact the stability and interaction with other molecules

Functional analysis of mutations

To elucidate the protein function and its association with other molecules, protein network analysis and interaction pattern has opened the avenues. Top 5 binding pockets predicted by GHECOM were graphically represented in Fig.5A.

Protein-protein network and interaction analysis

The STRING database exhibited 10 functional partners of SPTLC1, among which 8 were found with the confidence score >0.9 and two with score >0.99 (Fig. 5B and Table 6). Predicted interaction network has demonstrated that SPTLC2 and SPTLC3 were the strongest interaction partners with highest score ($c = 0.99$) (Fig. 5B and Table 6) and were shown to be involved in heterodimer formation with SPTLC1 protein. We pursued our analysis to investigate the SPTLC1 protein interaction upon binding to SPTLC2. Interacting residues of SPTLC1 with SPTLC2 protein are illustrated in Fig. 6.

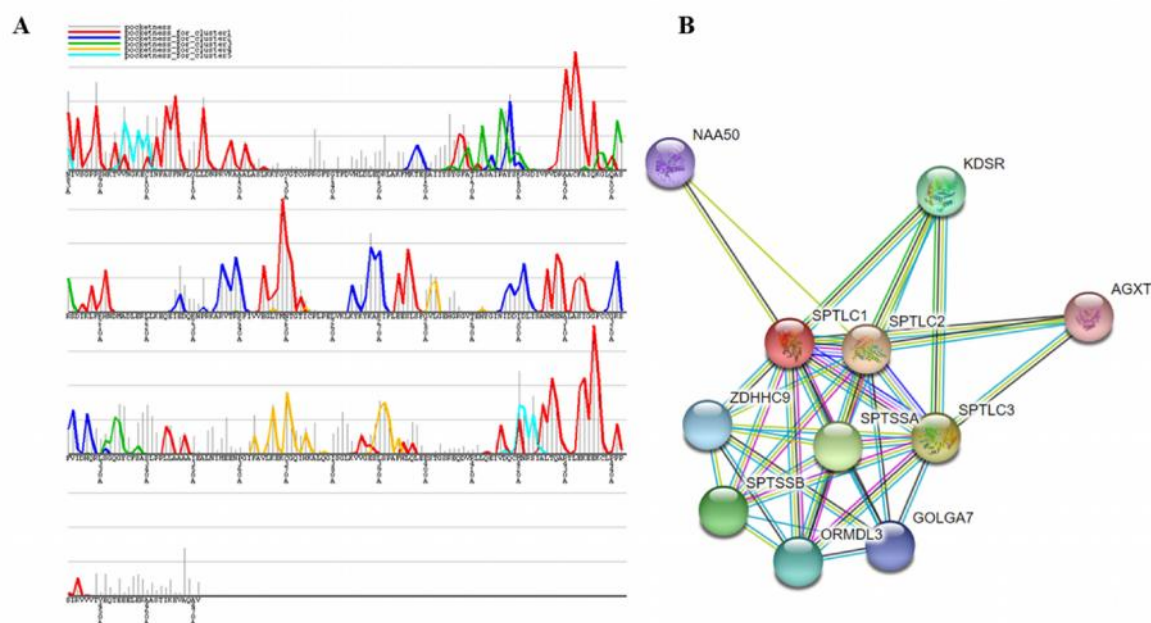


Fig. 5. Functional analysis of mutations. A: predicted multi-scale binding pockets on protein surface representation by GHECOM; B: functional protein network analysis. STRING interaction interwork show the association of SPTLC1 with different protein partners. In the above picture circles represent the one protein and the edges represent the protein-protein interactions.

Table 6. Predicted functional partners of SPTLC1 by STRING database.

Node 1	Node 2	Neighbourhood on chromosome	Phyloge netic cooccur rence	Homo logy	Co expre ssion	Experimental ly determined interaction	Data base annot ated	Automated Text mining	Combi ned score
SPTLC1	SPTLC2	0	0.526	0.74	0.27	0.925	0.9	0.931	0.996
SPTLC3	SPTLC1	0	0.526	0.733	0.27	0.921	0.9	0.928	0.995
SPTSSA	SPTLC1	0	0	0	0.049	0.329	0.9	0.864	0.99
SPTSSB	SPTLC1	0	0	0	0	0.329	0.9	0.864	0.99
KDSR	SPTLC1	0.09	0	0	0.092	0	0.9	0.652	0.967
ORMDL3	SPTLC1	0	0	0	0.128	0.462	0.9	0.282	0.961
ZDHHC9	SPTLC1	0	0	0	0.053	0	0.9	0.274	0.925
GOLGA7	SPTLC1	0	0	0	0.053	0	0.9	0	0.901
SPTLC1	NAA50	0	0	0	0.104	0	0	0.868	0.877
AGXT	SPTLC1	0	0	0	0.051	0	0.8	0.187	0.832

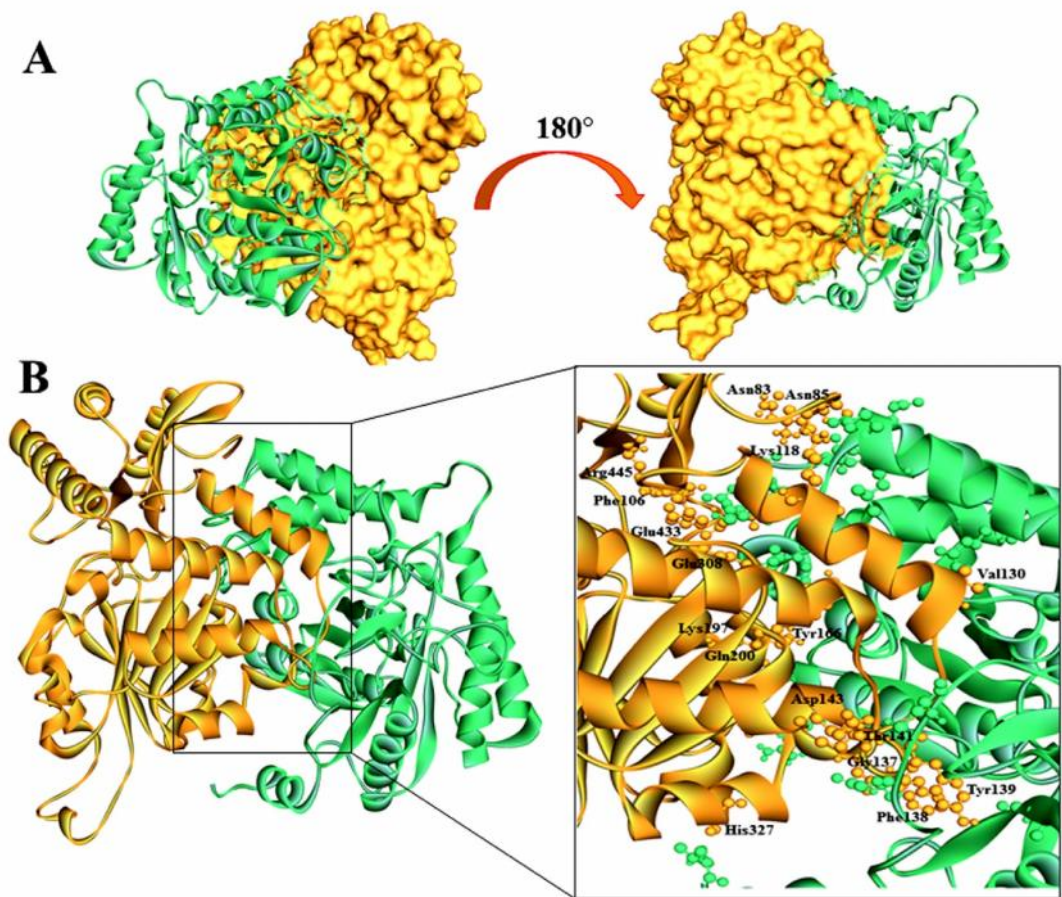


Fig. 5. Proposed binding interaction model between wild SPTLC1 and SPTLC2 reveals the active residues of wild SPTLC1 protein. Orange represents wild SPTLC1 while green represents SPTLC2. A: illustration of interacting model and binding pocket before and after 180° rotation; B: residues of wild SPTLC1 binding pocket involved in interaction are labelled.

Discussion

Due to the continuous discovery of genetic variations, experimentally delineation of the correlation of disease associated missense variants with underlying biological mechanism is demanding. Thus, in the era of computational biology, advanced *insilico* programs exhibit reliable approach in listing out the candidate genetic variants in accordance to their deleterious impact and consequence on structure and function of corresponding proteins. The concordant analysis of prediction programs increases the prediction accuracy, and thus reduces the false positive rate.

In the present study, computational screening was done using sequence and structure homology-based programs including SIFT and PolyPhen-2. Computational pathogenic variants prediction programs review has inferred that SIFT and PolyPhen has better execution power in identifying the pathogenic variants (47), likewise supported by Gnad et al., in 2013 (48). In addition, we also incorporated PROVEAN and MutPred results for our analysis. All missense mutations were further checked for disease association. Deleterious missense mutations predicted by three of the servers were selected. The destabilizing effect in majority of the deleterious mutations gives an indication about the disturbance in the structure and function of protein. Taking in consideration the above selection scheme, the selected mutations were screened from the data sets for further analysis (Table 1).

Among all selected missense mutations (Table 1), clinical and molecular consequences of some of the mutations have been reported previously (49-53). The variant p.S331F was found to be associated with early-onset and a severe HSAN phenotype (49, 50, 53). Additionally, p.C133W, p.C133Y and p.V144VD variations in SPTLC1 were the most examined missense mutations and observed to be the most widely recognized reason for HSAN-I (5, 51, 54, 55). Our concordant *in*

silico predictions for p.C133W, p.C133Y and p.V144D mutations also revealed the high deleterious effects (Table 1).

Prediction results of SIFT Indel Classifier and PROVEAN depicted frameshift variants and indels in coding sequence of *SPTLC1* as deleterious. Likewise, UTR variants were examined to search a variant in any functional pattern endorsed by UTRsite and UTR database. The 3'UTR contains the two different polyadenylation signals that mediate the poly (A) tail synthesis (56): nuclear polyadenylation signal (PAS) and CPE element.

Native human SPTLC1 model built by homology modeling based on 3a2b.1.A template shows the good overall quality and stereo-chemical properties. Protein relative solvent accessibility gives a protein structural and functional insight (57) as due to a residual mutation the solvent accessibility can be decreased, affecting protein stability. On average, disease causing variants that are likely to destabilize the protein reside mostly at the buried region of protein (58). In our analysis, most of the identified mutant residues belonged to the buried region of protein (Table 5) except Ser331. It has also been observed that the mutated residues belonged to the serine C-palmitoyltransferase activity domain and the structural difference of amino acids revealed that substituted residues have explicit properties like size, shape, density, and charges (Fig. 4B), and thus will impact the stability and interaction with other molecules.

Predicted interaction network demonstrated that SPTLC2 and SPTLC3 were the strongest interaction partners. The SPTLC1-SPTLC2-SPTSSA complex expresses a strong preference for C16-CoA substrate, while SPTLC1-SPTLC3-SPTSSA complex uses both C14-CoA and C16-CoA substrate, with slight preference for C14-CoA (59). A study shows that *SPTLC1* mutations induce a shift in SPT substrate specificity that leads to the formation of atypical non-degradable neurotoxic

sphingolipid metabolites resulting in HSAN-I (13). Study has also revealed the importance of disease-causing mutations in the active site of SPT that alters the relative positions of hydrophobic residues of both SPTLC1 and SPTLC2 subunits at dimer interface, thus affecting the enzyme activity (9, 60). Hence, it is certainly estimated that the enzymatic action of SPT would be influenced by the mutations either through the allosteric property of protein or the disturbance in the geometry of key residues present within the active site of enzyme that contributes in the recognition of substrate, or through the inadequate dimerization of the SPT monomers (61). It has been reported that in p.C133W, p.C133CY and p.V144D model, these amino acid residues do not specifically interact with the coenzyme or the substrate but lie at two closures of the loop that contact the other monomer to retain the dimer structure (61). Our study also shows that these selected residues also do not directly contact with SPTLC2 protein, but may be present around the interacting residues (Fig. 6).

Many previous comprehensive studies have shown the efficacy of consolidated computational programs for sorting detrimental variants from huge dataset (62-68). Previous studies have mentioned several physiological alterations in *SPTLC1* mutant cells, including a rise in both ER stress and potential oxidative phosphorylation (13, 14). Thus, in this study, we systematically demonstrated the computational investigation of SPTLC1 variants to study the aberrant effect of most deleterious variants affecting the structural and functional properties of protein.

In the study, we demonstrated a bioinformatics-based strategy for prioritizing the potentially functional SNPs from enormous set of polymorphisms. It proposes that the combination of various computational tools may impart an alternative approach that could opt for targeting SNPs. However, the functional consequence of candidate SNPs was not experimentally evaluated.

We believe that in future our provided prioritized list of potentially deleterious variants will be helpful for determine the contribution of key SNPs in disease progression.

Acknowledgments

We are sincerely grateful to Fatima Darakhshan for her essential help in improving the manuscript and assisting in critical writing.

Conflict of interest

The authors declare that they have no conflict of interest.

References

1. Merrill AH, Jr. Sphingolipid and glycosphingolipid metabolic pathways in the era of sphingolipidomics. *Chem Rev* 2011;111:6387-422.
2. Hanada K. Serine palmitoyltransferase, a key enzyme of sphingolipid metabolism. *Biochim Biophys Acta* 2003;1632:16-30.
3. Yard BA, Carter LG, Johnson KA, et al. The structure of serine palmitoyltransferase; gateway to sphingolipid biosynthesis. *J Mol Biol* 2007;370:870-86.
4. Alexaki A, Clarke BA, Gavrilova O, et al. De Novo Sphingolipid Biosynthesis Is Required for Adipocyte Survival and Metabolic Homeostasis. *J Biol Chem* 2017;292:3929-39.
5. Gable K, Han G, Monaghan E, et al. Mutations in the yeast LCB1 and LCB2 genes, including those corresponding to the hereditary sensory neuropathy type I mutations, dominantly inactivate serine palmitoyltransferase. *J Biol Chem* 2002;277:10194-200.
6. Bejaoui K, Wu C, Scheffler MD, et al. SPTLC1 is mutated in hereditary sensory neuropathy, type 1. *Nat Genet* 2001;27:261-2.
7. Verhoeven K, Timmerman V, Mauko B, et al. Recent advances in hereditary sensory and autonomic neuropathies. *Curr Opin Neurol* 2006;19:474-80.
8. Dawkins JL, Hulme DJ, Brahmabhatt SB, et al. Mutations in SPTLC1, encoding serine palmitoyltransferase, long chain base subunit-1, cause hereditary sensory neuropathy type I. *Nat Genet* 2001;27:309-12.
9. Gable K, Gupta SD, Han G, et al. A disease-causing mutation in the active site of serine palmitoyltransferase causes catalytic promiscuity. *J Biol Chem* 2010;285:22846-52.

10. Bode H, Bourquin F, Suriyanarayanan S, et al. HSAN1 mutations in serine palmitoyltransferase reveal a close structure-function-phenotype relationship. *Hum Mol Genet* 2016;25:853-65.
11. Eichler FS, Hornemann T, McCampbell A, et al. Overexpression of the wild-type SPT1 subunit lowers desoxysphingolipid levels and rescues the phenotype of HSAN1. *J Neurosci* 2009;29:14646-51.
12. Penno A, Reilly MM, Houlden H, et al. Hereditary sensory neuropathy type 1 is caused by the accumulation of two neurotoxic sphingolipids. *J Biol Chem* 2010;285:11178-87.
13. Myers SJ, Malladi CS, Hyland RA, et al. Mutations in the SPTLC1 protein cause mitochondrial structural abnormalities and endoplasmic reticulum stress in lymphoblasts. *DNA Cell Biol* 2014;33:399-407.
14. Stimpson SE, Coorssen JR, Myers SJ. Mitochondrial protein alterations in a familial peripheral neuropathy caused by the V144D amino acid mutation in the sphingolipid protein, SPTLC1. *J Chem Biol* 2015;8:25-35.
15. Stimpson SE, Coorssen JR, Myers SJ. Proteome alterations associated with the V144D SPTLC1 mutation that causes hereditary sensory neuropathy-I. *eJBio* 2015;11:176-86.
16. Stimpson SE, Lauto A, Coorssen JR. Isolation and identification of ER associated proteins with unique expression changes specific to the V144D SPTLC1 mutations in HSN-I. *Biochem Anal Biochem* 2016;5.
17. Stimpson SE, Shanu A, Coorssen JR. Identifying unique protein alterations caused by SPTLC1 mutations in a transfected neuronal cell model. *World J Neurosci* 2016;6:325-47.
18. Sherry ST, Ward MH, Kholodov M, et al. dbSNP: the NCBI database of genetic variation. *Nucleic Acids Res* 2001;29:308-11.
19. Zerbino DR, Achuthan P, Akanni W, et al. Ensembl 2018. *Nucleic Acids Res* 2018;46:D754-D61.
20. Hamosh A, Scott AF, Amberger JS, et al. Online Mendelian Inheritance in Man (OMIM), a knowledgebase of human genes and genetic disorders. *Nucleic Acids Res* 2005;33:D514-7.
21. Ng PC, Henikoff S. Predicting deleterious amino acid substitutions. *Genome Res* 2001;11:863-74.
22. Ng PC, Henikoff S. SIFT: Predicting amino acid changes that affect protein function. *Nucleic Acids Res* 2003;31:3812-4.
23. Kumar P, Henikoff S, Ng PC. Predicting the effects of coding non-synonymous variants on protein function using the SIFT algorithm. *Nat Protoc* 2009;4:1073-81.
24. Adzhubei IA, Schmidt S, Peshkin L, et al. A method and server for predicting damaging missense mutations. *Nat Methods* 2010;7:248-9.
25. Choi Y, Chan AP. PROVEAN web server: a tool to predict the functional effect of amino acid substitutions and indels. *Bioinformatics* 2015;31:2745-7.
26. Choi Y, Sims GE, Murphy S, et al. Predicting the functional effect of amino acid substitutions and indels. *PLoS One* 2012;7:e46688.
27. Li B, Krishnan VG, Mort ME, et al. Automated inference of molecular mechanisms of disease from amino acid substitutions. *Bioinformatics* 2009;25:2744-50.
28. Hu J, Ng PC. SIFT Indel: predictions for the functional effects of amino acid insertions/deletions in proteins. *PLoS One* 2013;8:e77940.
29. Mignone F, Grillo G, Licciulli F, et al. UTRdb and UTRsite: a collection of sequences and regulatory motifs of the untranslated regions of eukaryotic mRNAs. *Nucleic Acids Res* 2005;33:D141-6.
30. Grillo G, Turi A, Licciulli F, et al. UTRdb and UTRsite (RELEASE 2010): a collection of sequences and regulatory motifs of the untranslated regions of eukaryotic mRNAs. *Nucleic Acids Res* 2010;38:D75-80.
31. Arnold K, Bordoli L, Kopp J, et al. The SWISS-MODEL workspace: a web-based environment for protein structure homology modelling. *Bioinformatics* 2006;22:195-201.
32. Kiefer F, Arnold K, Kunzli M, et al. The SWISS-MODEL Repository and associated resources. *Nucleic Acids Res* 2009;37:D387-92.
33. Guex N, Peitsch MC, Schwede T. Automated comparative protein structure modeling with SWISS-MODEL and Swiss-PdbViewer: a historical perspective. *Electrophoresis* 2009;30 Suppl 1:S162-73.
34. Biasini M, Bienert S, Waterhouse A, et al. SWISS-MODEL: modelling protein tertiary and quaternary structure using evolutionary information. *Nucleic Acids Res* 2014;42:W252-8.
35. Colovos C, Yeates TO. Verification of protein structures: patterns of nonbonded atomic interactions. *Protein Sci* 1993;2:1511-9.
36. Lovell SC, Davis IW, Arendall WB, 3rd, et al. Structure

validation by Calpha geometry: phi,psi and Cbeta deviation. *Proteins* 2003;50:437-50.

37. Wiederstein M, Sippl MJ. ProSA-web: interactive web service for the recognition of errors in three-dimensional structures of proteins. *Nucleic Acids Res* 2007;35:W407-10.

38. Kaplan W, Littlejohn TG. Swiss-PDB Viewer (Deep View). *Brief Bioinform* 2001;2:195-7.

39. Cheng J, Randall A, Baldi P. Prediction of protein stability changes for single-site mutations using support vector machines. *Proteins* 2006;62:1125-32.

40. Petersen B, Petersen TN, Andersen P, et al. A generic method for assignment of reliability scores applied to solvent accessibility predictions. *BMC Struct Biol* 2009;9:51.

41. Rost B, Yachdav G, Liu J. The PredictProtein server. *Nucleic Acids Res* 2004;32:W321-6.

42. Yang J, Wang Y, Zhang Y. ResQ: An Approach to Unified Estimation of B-Factor and Residue-Specific Error in Protein Structure Prediction. *J Mol Biol* 2016;428:693-701.

43. Kawabata T. Detection of multiscale pockets on protein surfaces using mathematical morphology. *Proteins* 2010;78:1195-211.

44. Szklarczyk D, Morris JH, Cook H, et al. The STRING database in 2017: quality-controlled protein-protein association networks, made broadly accessible. *Nucleic Acids Res* 2017;45:D362-D8.

45. van Zundert GCP, Rodrigues J, Trellet M, et al. The HADDOCK2.2 Web Server: User-Friendly Integrative Modeling of Biomolecular Complexes. *J Mol Biol* 2016;428:720-5.

46. de Vries SJ, Bonvin AM. CPORT: a consensus interface predictor and its performance in prediction-driven docking with HADDOCK. *PLoS One* 2011;6:e17695.

47. Hicks S, Wheeler DA, Plon SE, et al. Prediction of missense mutation functionality depends on both the algorithm and sequence alignment employed. *Hum Mutat* 2011;32:661-8.

48. Gnad F, Baucom A, Mukhyala K, et al. Assessment of computational methods for predicting the effects of missense mutations in human cancers. *BMC Genomics* 2013;14 Suppl 3:S7.

49. Rothier A, Baets J, De Vriendt E, et al. Genes for hereditary sensory and autonomic neuropathies: a genotype-phenotype correlation. *Brain* 2009;132:2699-711.

50. Rothier A, Penno A, Rautenstrauss B, et al. Characterization

of two mutations in the SPTLC1 subunit of serine palmitoyltransferase associated with hereditary sensory and autonomic neuropathy type I. *Hum Mutat* 2011;32:E2211-25.

51. Davidson G, Murphy S, Polke J, et al. Frequency of mutations in the genes associated with hereditary sensory and autonomic neuropathy in a UK cohort. *J Neurol* 2012;259:1673-85.

52. Auer-Grumbach M, Bode H, Pieber TR, et al. Mutations at Ser331 in the HSN type I gene SPTLC1 are associated with a distinct syndromic phenotype. *Eur J Med Genet* 2013;56:266-9.

53. Suh BC, Hong YB, Nakhro K, et al. Early-onset severe hereditary sensory and autonomic neuropathy type 1 with S331F SPTLC1 mutation. *Mol Med Rep* 2014;9:481-6.

54. Bejaoui K, Uchida Y, Yasuda S, et al. Hereditary sensory neuropathy type 1 mutations confer dominant negative effects on serine palmitoyltransferase, critical for sphingolipid synthesis. *J Clin Invest* 2002;110:1301-8.

55. Dedov VN, Dedova IV, Merrill AH, Jr., et al. Activity of partially inhibited serine palmitoyltransferase is sufficient for normal sphingolipid metabolism and viability of HSN1 patient cells. *Biochim Biophys Acta* 2004;1688:168-75.

56. Barrett LW, Fletcher S, Wilton SD. Regulation of eukaryotic gene expression by the untranslated gene regions and other non-coding elements. *Cell Mol Life Sci* 2012;69:3613-34.

57. Wu W, Wang Z, Cong P, et al. Accurate prediction of protein relative solvent accessibility using a balanced model. *BioData Min* 2017;10:1.

58. Gong S, Blundell TL. Structural and functional restraints on the occurrence of single amino acid variations in human proteins. *PLoS One* 2010;5:e9186.

59. Schuster-Bockler B, Bateman A. Protein interactions in human genetic diseases. *Genome Biol* 2008;9:R9.

60. Raman MC, Johnson KA, Yard BA, et al. The external aldimine form of serine palmitoyltransferase: structural, kinetic, and spectroscopic analysis of the wild-type enzyme and HSN1 mutant mimics. *J Biol Chem* 2009;284:17328-39.

61. Ikushiro H, Islam MM, Okamoto A, et al. Structural insights into the enzymatic mechanism of serine palmitoyltransferase from *Sphingobacterium multivorum*. *J Biochem* 2009;146:549-62.

62. Sreevishnupriya K, Chandrasekaran P, Senthilkumar A, et al. Computational analysis of deleterious missense mutations in

aspartoacylase that cause Canavan's disease. *Sci China Life Sci* 2012;55:1109-19.

63. Masoodi TA, Alsaif MA, Al Shammari SA, et al. Evaluation and identification of damaged single nucleotide polymorphisms in COL1A1 gene involved in osteoporosis. *Arch Med Sci* 2013;9:899-905.

64. Hussain MRM, Nasir J, Al-Aama JY. Clinically significant missense variants in human GALNT3, GALNT8, GALNT12, and GALNT13 genes: intriguing in silico findings. *J Cell Biochem* 2014;115:313-27.

65. Naveed M, Tehreem S, Mubeen S. In-silico analysis of non-synonymous-SNPs of STEAP2: To provoke the progression of

prostate cancer. *Open Life Sci* 2016;11:402-16.

66. Solayman M, Saleh MA, Paul S, et al. In silico analysis of nonsynonymous single nucleotide polymorphisms of the human adiponectin receptor 2 (ADIPOR2) gene. *Comput Biol Chem* 2017;68:175-85.

67. Sadaf T, Darakhshan F. Identification of Deleterious Nssnps of Interleukin-2 (IL-2) Gene and Its Structural Stability Using Computational Methods. *Int J Res* 2018;5:131-50.

68. Alipoor B, Ghaedi H, Omrani MD, et al. A Bioinformatics Approach to Prioritize Single Nucleotide Polymorphisms in TLRs Signaling Pathway Genes. *Int J Mol Cell Med* 2016;5:65-79.